Hindawi
Journal of Advanced Transportation
Volume 2022, Article ID 5985542, 13 pages
https://doi.org/10.1155/2022/5985542

Research Article

Seismic Analysis of Reticulated Shell Structure Based on Sensor Network for Smart Transportation Seismic Isolation Bearings

Jun Peng and Yufei Li

College of Agricultural and Hydraulic Engineering, Suihua University, Suihua 152001, Heilongjiang, China

Correspondence should be addressed to Jun Peng; 171841220@masu.edu.cn

Received 18 February 2022; Revised 19 March 2022; Accepted 31 March 2022; Published 22 April 2022

Academic Editor: Sang-Bing Tsai

Earthquakes are one of the most frequent and inevitable natural disasters that occur on Earth. The most important seismic isolation device used in the isolation technology is the isolation bearing, but the limited structure of the isolation bearing is not suitable for the seismic isolation and shock absorption of smart transportation buildings. Therefore, it is very important to improve the new generation of seismic isolation structures with good seismic isolation effect, stable performance, and economical performance. It is very important to study the structural composition of the isolation bearing and the rigidity of the isolation structure. Isolation bearings are designed to resist and absorb the energy of seismic shocks by installing substructures in the structure. Active control involves installing sensors on the structure and its foundation to determine how the structure responds to seismic action. In this paper, based on the intelligent transportation of the sensor network, the reticulated shell structure of the isolation bearing is analyzed. By introducing the architecture and network layout of the sensor network, it is beneficial to obtain more accurate seismic data in complex and difficult terrain. This paper analyzes the technical principle of seismic isolation technology, which can effectively avoid the upward transmission of ground vibration by increasing the flexibility and proper damping of the system. From the experimental data of the seismic response of the ground-isolated structure to the near-field pulsation and far-field vibration, the total energy of the ground-isolated structure under the near-field pulsed ground motion is the largest. The seismic isolation effect of the reticulated shell structure of the seismic isolation bearing prevents more than 80% of the seismic energy from being transmitted to the superstructure.

1. Introduction

Over the past three decades, China's economy has boomed and the construction of large-scale technical buildings has achieved remarkable results. The emergence of large-scale transportation facilities with various large volumes and complex spatial forces makes the seismic behavior of these large-scale buildings in the event of earthquakes very important. In order to improve the seismic behavior of space structures, researchers began to introduce the theory of seismic isolation of space structures and initially developed seismic load reduction and isolation technologies for such structures. The traditional seismic design resists the seismic action of the structure's own bearing capacity, stiffness, and flexibility, that is, relying on the structure itself to consume seismic energy, which is uneconomical and cannot achieve the desired effect. At present, people have turned their attention to seismic isolation research, and domestic and foreign structural shock absorption and seismic isolation technologies have developed rapidly.

Large-scale spatial structures have developed rapidly in recent decades. Large space structure is not only a structural system for large space structures, such as large stadiums and hangars but also widely used in large public buildings, such as transportation hubs and conference centers. With the development of the national economy and the improvement of infrastructure, the demand for large profile structures is increasing every day. However, most structures are flexible systems with low damping ratios, which cause relatively high vibrations under dynamic loads, affecting the normal use of

the structure, which in turn affects safety. The study found that the use of seismic isolation technology or adding damping devices to the structure can effectively reduce the degree of damage to building facilities caused by earthquakes. China is geographically located in an earthquake-prone area. Large buildings often have a large number of people, and the personal and property losses caused by earthquakes may be huge. Therefore, the seismic behavior of large spatial structures is a topic that structural designers and researchers need to consider.

This paper is based on isolation technology to reduce the loss caused by the earthquake. The earthquake-isolated traffic building can effectively reduce the damage to the superstructure in the earthquake disaster, thereby greatly reducing the maintenance and repair costs after the earthquake. In the reticulated shell structure management model of the intelligent transportation isolation bearing, the intelligent transportation model based on the sensor network is adopted and combined with the road traffic conditions, such as the traffic flow speed, road characteristics, and other guidance models, network data is collected to realize the intelligent transportation operation.

2. Related Work

Wu Q conducted a high deformation horizontal displacement test on LRB600 and LRB1100 (LRB600, LRB1100: vibration isolation rubber bearing), and the deformation index was 400%. The results show that the bending stiffness after installation increases when the displacement strain reaches 240%, the hardening stiffness increases with the displacement strain, and when the displacement strain reaches 400%, the hardening stiffness increases by a factor of 1.5. He compared the seismic response, elastoplastic response spectrum, and plastic energy dissipation state of LRB of the traditional bilinear model and the proposed multilinear model, respectively. The results show that for large earthquakes, the hardening of the bearing weakens the seismic isolation capability of the LRB, the acceleration of the superstructure increases by 30%–50%, and the plastic energy dissipation of the structure increases, and the superstructure enters a state of plastic deformation. Therefore, without considering the hardening of the supports, the seismic response of the structure will be underestimated [1]. Hong et al. present a framework for seismic analysis of high-speed interconnected bridge systems with pendulum friction bearing isolation. Using computer simulation techniques, he performed dynamic simulations of seismic isolation systems for five railway bridges under seismic conditions. He considered a 35-degree-of-freedom (DOF) train consisting of eight 4-axle passenger cars and modeled the FPB with force elements including nonlinear spring and damper properties and hysteresis functions. The results show that replacing CSB with FPB with a friction coefficient of not less than 0.05 can greatly reduce the dynamic response of the train [2]. Recently, the number of base-isolated buildings for general commercial buildings is increasing due to the high seismic performance of the seismic isolation system. On the other hand, for nuclear power plants (NPPs), although there has been a lot of research to apply isolation systems, no plants for base isolation have been built in Japan. Recent seismic regulations require an assessment of seismic safety, including the eventual conduct of national nuclear power plants. Therefore, the final behavior of national nuclear power plants employing seismic isolation systems must also take into account the residual risk of earthquakes: for example, hardening in horizontal deformation or rupture of seismic isolators. The seismic response prediction method based on energy balance and its design method will be regarded as the seismic safety evaluation of large horizontal deformation area. Hiraki et al. especially proposed a mechanical energy balance evaluation scheme for studying the extreme behavior of large deflection regions, which can estimate the mechanical energy conversion based on the experimental records of the relationship restoring force and shear deflection on the base isolation layer. However, it has not been widely used [3]. The seismic capacity and continuous operation of bridges after earthquakes are important seismic design criteria. Mohebbi et al. explore a new concept for seismic protection of monolithic piers that uses sliding bearings to separate the superstructure from the piers. The effect of sliding bearings on the seismic response of a representative 3-span monolithic highway bridge is investigated. By sliding the bearing, the shear force of the pier is limited to the design friction of the bearing. Furthermore, since the displacement requirement of the bridge is governed by the equal displacement rule, it was found that the ductility requirement of the bridge pier is not sensitive to the friction force of the sliding bearing [4]. In order to solve the problem of three-dimensional isolation of high-rise buildings, Yan et al. introduced the prototype structure, model structure, and vibration test system. He conducted vibration tests and showed that although the three-dimensional vibration isolation bearings placed at the bottom of the substructure differed in the shape and damping mechanism of the vibration isolation, the natural vibration period of the structure was prolonged both horizontally and vertically. The simulation results are consistent with the experimental results. The isolated base structure has an obvious damping effect on the seismic response of the main structure of different groups [5]. Qingning et al. applied friction-slip isolation theory to study the seismic isolation performance of curved bridges. He studied the relationship between stress, strain, and displacement of rubber friction-slip isolation under two typical working conditions, established the constitutive slip-friction relationship, and obtained and analyzed the friction-slip calculation method and energy dissipation mechanism. Combined with shaking table test, the effects of different types of seismic waves and different acceleration loads on the failure state and seismic isolation effect of bridge piers with different stiffness are analyzed. The research shows that the cracks in the drawings are mainly flexible cracks, and the stiffness of the drawings has a greater influence on the crack position; the bearing is mainly damaged by shearing. In a strong earthquake, the acceleration response of the bearing is basically independent of the type of seismic wave but related to the friction coefficient between the bearing and the bearing. Moreover, the effect of

friction-slip isolation bearings increases with the loading level [6]. Wireless sensor networks (WSNs) are an important technology for the Internet of Things (IoT) and smart applications. In intelligent transportation systems (ITS), WSNs play an important role in safe and efficient traffic management. Therefore, there is a huge demand for energy-efficient WSNs with dynamic resource allocation in vehicles and infrastructure. Mukherjee A proposed a model of multiple-input multiple-output (MIMO) technology in WSNs to solve the problem of cluster head (CH) identification for MIMO sensor networks by using a back-propagation neural network (BPNN). Due to the influence of dynamic and real-time environments, traditional CH identification has the problem of insufficient location identification. Therefore, in order to obtain more precise localization accuracy, the proposed work uses BPNN combined with distributed gradient descent technique to calculate the location of unknown CH. This reduces distance estimation errors and further uses particle swarm optimization techniques to obtain optimal weights and thresholds for the network. The advantage of particle swarm optimization is that it is simple and easy to implement, and there are not many parameters to adjust. This work is validated through mathematical analysis, simulations, and comparisons with the state-of-the-art [7]. The above studies provide a detailed analysis of the seismic isolation capability and the application of sensor networks. It is undeniable that these studies have greatly promoted the development of the corresponding fields. We can learn a lot from methodology and data analysis. However, in the field of intelligent transportation, there are relatively few studies on the reticulated shell structure of the isolation bearing, and it is necessary to fully apply these theories to the research in this field.

3. Combination Analysis of the Smart Transportation of Sensor Network and the Reticulated Shell Structure of the Isolation Bearing

Earthquakes are sudden and heavy-weight disasters that cause heavy economic losses and casualties. Located between the Asia-Europe earthquake zone and the Pacific Rim region, China is a country with frequent seismic activities and many seismic waves. Seismic waves are vibrations propagating from the source of the earthquake in all directions and refer to the elastic waves that are generated from the source and radiate to the surroundings. Seismic waves appear in strong objects after being perceived by the source and have various properties [8]. Seismic waves can be divided into two categories according to their performance range, namely surface waves and body waves, and body waves are further divided into longitudinal waves (P waves) and transverse waves (S waves).

In seismology, the wave impedance is the product of the density of the medium and the velocity of the wave. The wave impedance is related to the radiation source. The radiation source is low impedance, and the electromagnetic wave generated is also low impedance, and vice versa. The wave impedance is also related to the distance from the observation point to the radiation source. When the distance is greater than 1/6 of the wavelength, the wave impedance is 377 ohms regardless of the radiation source impedance. And the distance between the radiation source and the radiation source is less than 1/6 wavelength is called the near field area, and the far field area is more than 1/6 wavelength. The wave impedance affects the motion of the wave and the state of wave propagation at the boundary between the two media. Table 1 shows wavelength propagation rates and wave impedance reference values for different regions [9].

The complexity of the subsurface structure and the existence of many unstable boundaries in the near-surface environment and the fact that the media parameters may be different in different regions mean that the propagation velocity of seismic waves in the subsurface is not consistent [10].

3.1. The Main Structure of Unconstrained Concrete. Concrete materials used in structural models can be divided into constrained concrete and unconstrained concrete. The stress-strain curve under uniaxial loading of unconstrained concrete can be determined by the following formula:

$$\begin{aligned}
\sigma &= (1 - e_c) F_c \varepsilon, \\
e_c &= \begin{cases} 1 - \dfrac{\rho_c m}{m + x^m - 1}, & x \le 1, \\ 1 - \dfrac{\rho_t}{\varphi_c (x - 1)^2 + x}, & x > 1, \end{cases} \\
x &= \frac{\varepsilon}{\varepsilon_{c,r}}, \\
\rho_c &= \frac{e_{c,r}}{F_c \varepsilon_{c,r}}, \\
m &= \frac{F_c \varepsilon_{c,r}}{F_c \varepsilon_{c,r} - e_{c,r}}.
\end{aligned} \tag{1}$$

Among them, φ_c is the value of the descending part of the concrete compressive strength curve; $e_{c,r}$ is the representative value of the concrete compressive strength. $\varepsilon_{c,r}$ is the maximum value of concrete compressive strength corresponding to the compressive strength $e_{c,r}$ value; e_c is the failure evolution parameter of concrete compressive strength.

3.2. Constrained Concrete Main Structure. Confined concrete can solve the shortcomings of crack width development, easy crushing, and poor ductility of concrete members. Confined concrete can also be divided into reinforced concrete and stirrup concrete. Concreting uses external constraints to improve its original compressive properties and compressive strength and ductility. High-strength stirrups are used in the beams, columns, nodes, and hoops in the walls of concrete structures to constrain the

Table 1: Propagation speed and wave impedance of waves in different media.

Media name	Rock layer	Soil	Clay	Limestone
Speed (m/s)	300~13000	200~800	1800~2400	3200~5500
Density (kg/cm^3)	1.4~2	1.1~2	1.5~2.2	2.3~3
Wave impedance (g/s $*$ cm$^2 \times 10^4$)	4.2~26	2.2~16	27~52.8	73.6~165

concrete to form a constrained concrete structure system. And the uniaxial stress-strain curve of stirrup concrete is calculated according to the following formula:

$$
\begin{aligned}
e_c &= \frac{e'_{cc} xs}{s + x^s - 1},\\
x &= \frac{\varepsilon_c}{\varepsilon_{cc}},\\
\varepsilon_{cc} &= \varepsilon_{co}\left[5\left(\frac{e'_{cc}}{e'_{cc}} - 1\right) + 1\right],\\
s &= \frac{F_c}{F_c - F_{\sec}},\\
F_c &= 5000\sqrt{e'_{co}},\\
e'_{cc} &= e'_{co}\left(2.254\sqrt{1 + \frac{7.94e'_l}{e'_{co}}} - \frac{2e'_l}{e'_{co}} - 1.254\right).
\end{aligned}
\tag{2}
$$

Among them, e'_{cc} is the strength of the constrained concrete, $e'_{co}, \varepsilon_{co}$ is the compressive strength and the maximum strength of the unconstrained concrete, generally taking $\varepsilon_{co} = 0.002$; $F_c, F_{\sec}$ is the tangent modulus and secant modulus of the concrete.

The traditional seismic structure mainly uses the plastic deformation and energy dissipation of the main structure after yielding against lateral force to dissipate the force of the earthquake. In the structural design of building facilities, on the one hand, by reducing the bottom stiffness of the building structure, the effect of earthquakes on the building is reduced. On the other hand, it is to increase the interface of components, enhance the rigidity of the bottom of the structure, and improve the resistance of the building itself. The principle of seismic isolation technology is to increase the self-correction time of the system itself, thus exceeding the characteristic period of the object and the bearing time of the superstructure. By maintaining the flexibility of the system and good damping, the vibration to the ground is effectively avoided so that the upper system is in a flexible position and the safety of the system is ensured [11]. As the damping of the system increases, the vibration isolation efficiency gradually decreases, but with the increase of the frequency ratio, the vibration isolation efficiency increases. When the system damping increases, the equipment quality also has a certain influence on the vibration isolation efficiency. By prolonging the oscillation time of the system, according to the response scenario, the acceleration of the vibration is reduced, the distortion of the protected system under the action of the earthquake becomes no longer significant, and the response to the seismic force is reduced [12]. This is considered a key direction for future research, as it contributes more to the safety within system facilities than the usual simple design of system rigidity and function.

As the load-bearing member of the structural system, the main function of the bearing is to transmit the upper bearing force of the supporting structure and ensure the harmonious deformation of the upper and lower parts of the structure [13]. In the event of a sudden earthquake, the bearing is the direct part of the lower part where the seismic force is transmitted. Initially, the widely used steel bearings in the project failed to provide significant seismic isolation during large earthquakes, and the seismic forces were almost entirely transferred to the superstructure, resulting in complete structural failure [14].

The continuous evolution of structural design concepts and the continuous development of various building materials are conducive to the rapid development and application of large-frame buildings. Among them, the reticulated shell structure, as an important element of large-scale space structure, has gradually won the resonance of designers with its beautiful architectural form and has been used more and more widely [15]. The reticulated shell structure is a new type of space structure derived from thinness and characteristics. It is a net-like body based on rods, and the rods are formed according to certain rules. Its form is the structure of the organizer, forming the overall structure of the space frame. It has both the force transmission characteristics of the rod system and the structural characteristics of the shell. The force is mainly transmitted point-to-point through the two directions of tension, compression, or displacement in the shell, and the force transmission process is very clear [16].

At present, the commonly used shell structures at home and abroad are divided into single-layer shell structure, prestressed shell structure, ribbon cable support shell structure, single-layer fork-roll shell structure, etc. There are many forms of reticulated shell structures, such as spherical reticulated shells, hyperbolic plane reticulated shells, and hyperbolic, parabolic reticulated shells, which can be combined in various forms in the design [17]. This opens up a wide range of possibilities for designing buildings with large gaps to create different plan shapes and new unique architectural forms. It has been widely used in engineering practice due to its reasonable structural tension, high stiffness, low weight, beautiful and diverse shapes, and good technical and economic performance [18].

For the seismic isolation principle of reticulated shell structures, the structural oscillation control of spatial grids can be divided into three categories.

(1) The energy dissipation support system is located in the lower part of the structure.

(2) Dissipating energy and reduce vibration by installing isolation bearings, including sliding bearings and viscoelastic bearings.

(3) Installing dampers on the upper part of the reticulated shell structure for vibration isolation.

By reasonably arranging the seismic isolation bearings, the sliding bearings can form an effective seismic isolation layer. During the seismic activity, the sliding of the bearings and the expansion and contraction of the large coil springs will consume a certain amount of energy. At the same time, the self-sustained seismic period of the structure far from the optimal period of the site is prolonged, and the seismic response is weakened to a certain extent [19].

In order to make up for the high cost of lines, maintenance problems, expensive and difficult lines in the traditional wired seismic data acquisition system in the field, in the whole system design, wireless communication technology is chosen to replace the communication work using a large number of communication cables in the traditional seismic data acquisition system [20]. The use of wireless transmission solutions facilitates the distributed deployment of seismic measurement units and enables efficient seismic operations in complex terrain. Wireless data transmission includes data communication between the receiving computer and each receiving unit and network communication between adjacent wireless communication units [21]. Table 2 is a comparison of the main technical indicators of wireless communication technology.

As a self-organized and distributed network centered on data transmission and exchange, sensor network provides data from a large number of sensor nodes. Real-time monitoring, joint exchange of data and information, and transmission of monitoring data are enabled even under very difficult conditions [22]. Therefore, wireless sensor network has been widely used in many fields, and its use in earthquake monitoring can provide a more real and reliable information basis for earthquake prevention and rescue. A wireless sensor network consists of some randomly distributed sensor nodes, which together constitute a wireless sensor network architecture [23]. Sensor nodes are self-organizing and capable of monitoring objects in real-time, collecting information, and sending data wirelessly. Wireless sensor networks detect, collect, process, and transmit sensor data, which is their most basic function.

Wireless sensor network is a comprehensive intelligent system that integrates sensor technology, MEMS, embedded technology, network communication technology, and information computing technology [24]. The sensor network is configured and managed by the user through the control node. The data collected by the sensor node is transmitted to other sensor nodes in the form of jump connection through the network, and the control node provides monitoring and retrieval of monitoring data. The architecture of the sensor network is shown in Figure 1.

The sensor node consists of a sensor module, a processor module, a wireless communication module, and a power supply module, as shown in Figure 2. The sensor module is responsible for information collection and data transmission in the monitoring area [25]. The processor is usually an embedded processor. The wireless communication module is responsible for wireless communication with other parts of the system, exchanging control information, and sending and receiving data. The power supply unit provides the power needed to operate the sensor components and typically uses a small battery.

MEMS sensor is one of the earliest products widely used in commerce, and it is also one of the fastest growing technologies in MEMS technology. MEMS stands for Micro-Electro-Mechanical Systems, which are integrated devices or systems composed of electronic and mechanical components manufactured through large-scale processing processes, compatible with integrated circuits, and ranging in size from small to millimeters. In particular, it combines computers, sensors, and actuators to change the way nature is perceived and managed. Compared with traditional sensors, it has the characteristics of small size, light weight, low cost, low power, high reliability, suitable for mass production, easy integration, and intelligence. Its micro- or nanoscale size enables it to achieve some functions that traditional mechanical sensors cannot.

MEMS accelerometers are usually attached to an external object so that the motion of the object is represented by the motion of the accelerometer. When the accelerometer is accelerated together with an external object, the mass moves in the opposite direction under the influence of the inertial force acting on the spring. As shown in Figure 3(a), the spring and damper can quantify the motion of an object. The laws of physics show that there is a one-to-one correspondence between acceleration and displacement: as the acceleration changes, the displacement of the mass also changes, and the change in acceleration can be represented by the change in displacement. At the same time, it can be seen from Figure 3(b) that with the change of mass displacement, the capacitance between the stationary glass and the moving glass also changes accordingly. That is, C_{x_1} and C_{x_2} change due to the change of the distance between the plates, and the mathematical expression is as follows:

$$C_{x_1} = \frac{\varepsilon\varepsilon_0 S}{d - x},$$
$$C_{x_2} = \frac{\varepsilon\varepsilon_0 S}{d + x}. \tag{3}$$

Among them, C_{x_1} and C_{x_2}, respectively, represent the two capacitances between the fixed glass and the movable glass, where $\varepsilon_0 = 8.854 \times 10^{-12} F/m$ is the dielectric constant of the vacuum; ε is the relative permittivity of the medium between the plates, which is 1 in air; S is the covering area (m^2) of the plates; x is the displacement of the mass block, and d is the distance between the fixed glass and the movable glass.

The change in capacitance will be displayed by voltage, specifying V_p for the input voltage signal and V_s for the output voltage. The relationship between the output voltage and the input voltage is as follows:

Table 2: Comparison of main technical indicators of wireless communication technology.

Technical standards	Operating band	Transmission rate	Standby time	Transmission distance (m)	Main uses
WiFi	2.4 GHz	11 Mbps	1~6 hours	10~100	Wireless LAN
Bluetooth	2.4 GHz	1 Mbps	1~3 weeks	0~10	Personal network
ZigBee	868/915 MHz, 2.4 GHz	20~250 kbps	6~24 months	10~75	Sensor networks

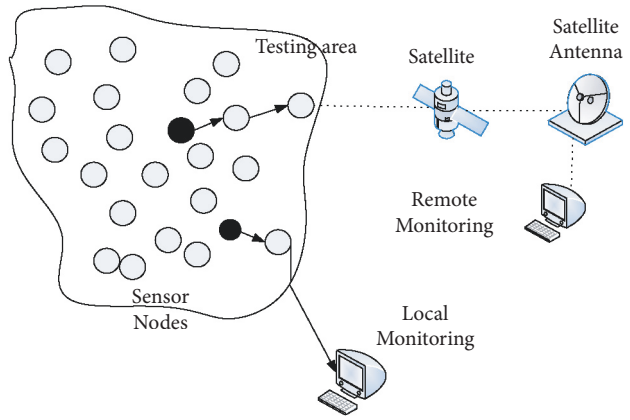

Figure 1: Architecture of a sensor network.

$$V_s = \frac{C_{x_1} - C_{x_2}}{C_{x_1} + C_{x_2}} V_p. \tag{4}$$

By measuring the change in voltage, the displacement change of the mass can be obtained. Voltage and displacement have a linear relationship, which is expressed as follows:

$$V_s = \frac{x}{d} V_p. \tag{5}$$

According to Newton's second law, the motion direction of the mass block is opposite to that of the object, and the relationship between the mass block displacement and acceleration is expressed as follows:

$$\begin{aligned} F &= kx \\ &= -ma, \end{aligned} \tag{6}$$

where k is the stiffness coefficient of the spring; m is the mass of the mass. Therefore, the relationship between the external acceleration and the output voltage is expressed as follows:

$$\begin{aligned} a &= \frac{kx}{m} \\ &= \frac{kdV_s}{mV_p}. \end{aligned} \tag{7}$$

It can be concluded from the above formula that there is a one-to-one correspondence between the acceleration and the output voltage, and the acceleration can be quantified by the change of the output voltage.

In view of the randomness and uncertainty of wireless seismic sensors in practical use, the P-wave components captured by seismic waves are biased. In this paper, a self-correction method of accelerometer position based on longitudinal wave measurement is proposed, which can automatically detect the rotation correction of installation direction and coordinates, and the corrected accelerometer can be used to eliminate the influence of sensor positioning.

The accelerator position correction method is divided into two parts: first, the data collected by the accelerator are compared and analyzed, a vertical axis is selected, and then the coordinate rotation on the selected axis is corrected, and the sensor data is self-corrected.

Sensor self-calibration method:

3.3. Identifying the Installation Direction and Selecting the Vertical Coordinate Axis. The simulation diagram of the sensor coordinate system is shown in Figure 4(a). During the installation process of the MEMS sensor, there is usually an included angle between the Z-axis and the gravitational acceleration. This is because a mass block is added to the acceleration sensor, so it will always be affected by gravity. As long as the measurement axis is not perpendicular to gravity, the inclination angle between the sensor and gravity can be measured. Let the included angle be θ. At this time, the gravitational acceleration will produce a projected component on the xyz coordinate axis. There is the following relation:

$$\cos\theta = \frac{g_r}{g}. \tag{8}$$

The axis with the smallest angle θ, that is, the axis with the largest gravitational acceleration projection, is chosen as the reference direction. Where g_x, g_y and g_z are the component modulus of the gravitational acceleration on the xyz axis, and g is the gravitational acceleration value at rest. r is the axial direction corresponding to the maximum value of g_x, g_y and g_z, ie the chosen reference direction. g_r is the modulus of the gravitational acceleration component on the reference axis.

3.4. Coordinate Rotation Correction. The coordinate rotation model is shown in Figure 4(b), where g is the gravitational acceleration at rest and g_r is the mode of the gravitational acceleration component on the reference axis. G is the acceleration value when the accelerometer moves after calibration, G_r is the acceleration value when the reference axis is selected, where

$$g = \sqrt{g_x^2 + g_y^2 + g_z^2}. \tag{9}$$

The accelerometer values at rest and in motion on the reference axis should be measured under conditions g_r and G_r, respectively. Since the angle between the reference axis and the gravitational acceleration is constant at rest and in

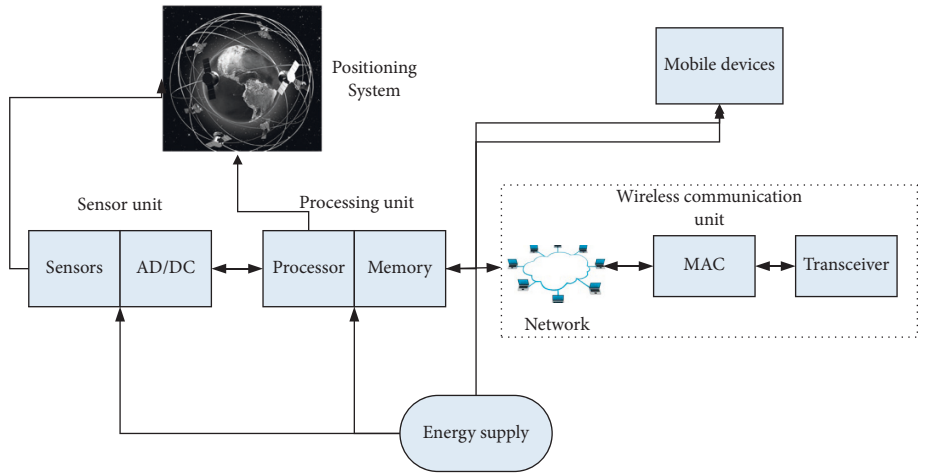

Figure 2: Node structure of the sensor.

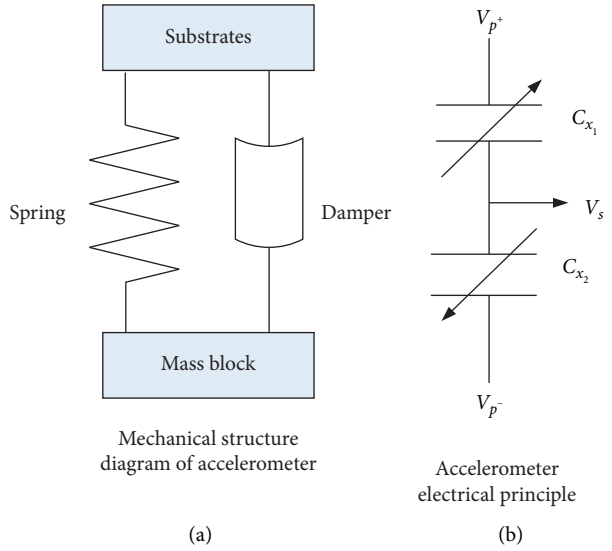

Figure 3: Schematic diagram of the working principle of accelerometer. (a) Mechanical structure diagram of accelerometer. (b) Accelerometer electrical principle.

motion, it can be concluded that the acceleration values at rest and in motion are also proportional. It follows that:

$$\cos\theta = \frac{g_r}{g} = \frac{G_r}{G}. \tag{10}$$

Corrected G value for accelerometer motion:

$$G = \frac{g}{g_r} G_r. \tag{11}$$

(g/g_r) is the correction coefficient in the above formula, which is used to adjust the collected data. The adjusted value deducts the value of the gravitational acceleration to obtain the actual value of the acceleration a, as shown in the following formula:

$$a = \frac{g}{g_r} G_r - g. \tag{12}$$

The above formulas allow for self-correction of the accelerometer position, which in turn translates the correction into more precise data, thereby eliminating the effect of the accelerometer position on seismic data acquisition. The accelerator position self-correction algorithm eliminates the influence of accelerator placement position, which is beneficial to the placement of wireless seismic sensors in the field, which can be used to obtain more accurate seismic data in complex terrain.

The sensor network first uses the physical layer of the data collection and transmission module to detect road traffic conditions, such as traffic flow speed, traffic flow size, lane occupancy, road characteristics, and other traffic indicators, as shown in Figure 5.

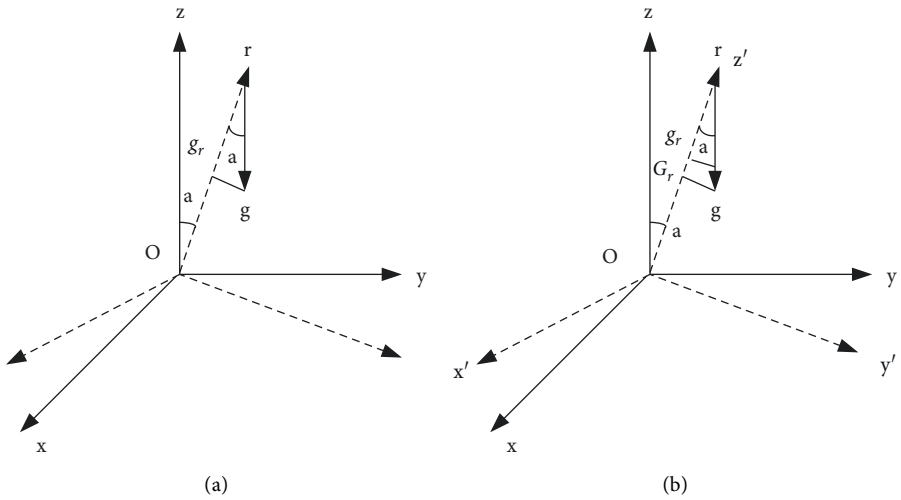

Figure 4: Simulation diagram of sensor coordinate system and schematic diagram of rotation model.

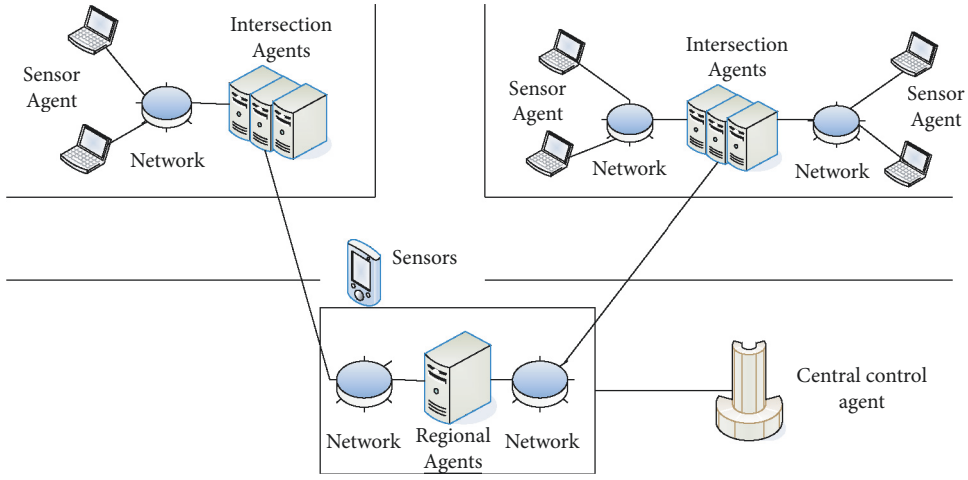

Figure 5: Network layout of the model.

Seismic sensor networks include detectors, differential low-pass filters for attenuating radio signals, amplifier circuits, low-pass filters, A/D conversion circuits, microprocessors, and data storage units. The detector is used to detect the vibration signal and convert it into a voltage regulation; since the RF signal appears as a DC distortion output in the area where the RF signal is strong, different low frequency parameters are used to reduce the interference of the RF signal. The signal output is not very strong, so it is very important to design the same amplifier circuit, which is mainly used to increase the reception of the small signal of the sensor, and the frequency of the vibration signal caused by the human body or the vehicle is lower than 150 Hz. To prevent noise signals from entering the A/D module (analog-to-digital conversion), the filter circuit behind the built-in amplifier circuit is low-pass, and the power control module provides a stable power supply with low ripple factor. Figure 6 is a schematic diagram of the sensor network application function.

As can be seen from Figure 6, the sensor output signal goes through the delay mode and then enters the A/D for data conversion, and another signal enters the comparator, and the output of the comparator is used as an external signal. Another approach to system optimization is to set thresholds in the node detection software and use the results to compare the A/D-evaluated values to the thresholds. When the excitation system is executed, the received data is stored in memory as valid data. The memory is used to store the data after A/D conversion. After the assembly process is completed, the CC2530-based wireless transceiver reads the data and sends it to the sink node. A/D data retrieval, memory read and write, and signal detection are all implemented by FPGA.

4. Seismic Experimental Design of Reticulated Shell Structure for Isolation Bearings

The analytical model is a double-layer spherical reticulated shell structure with a span arrangement of 60 meters, a rise-

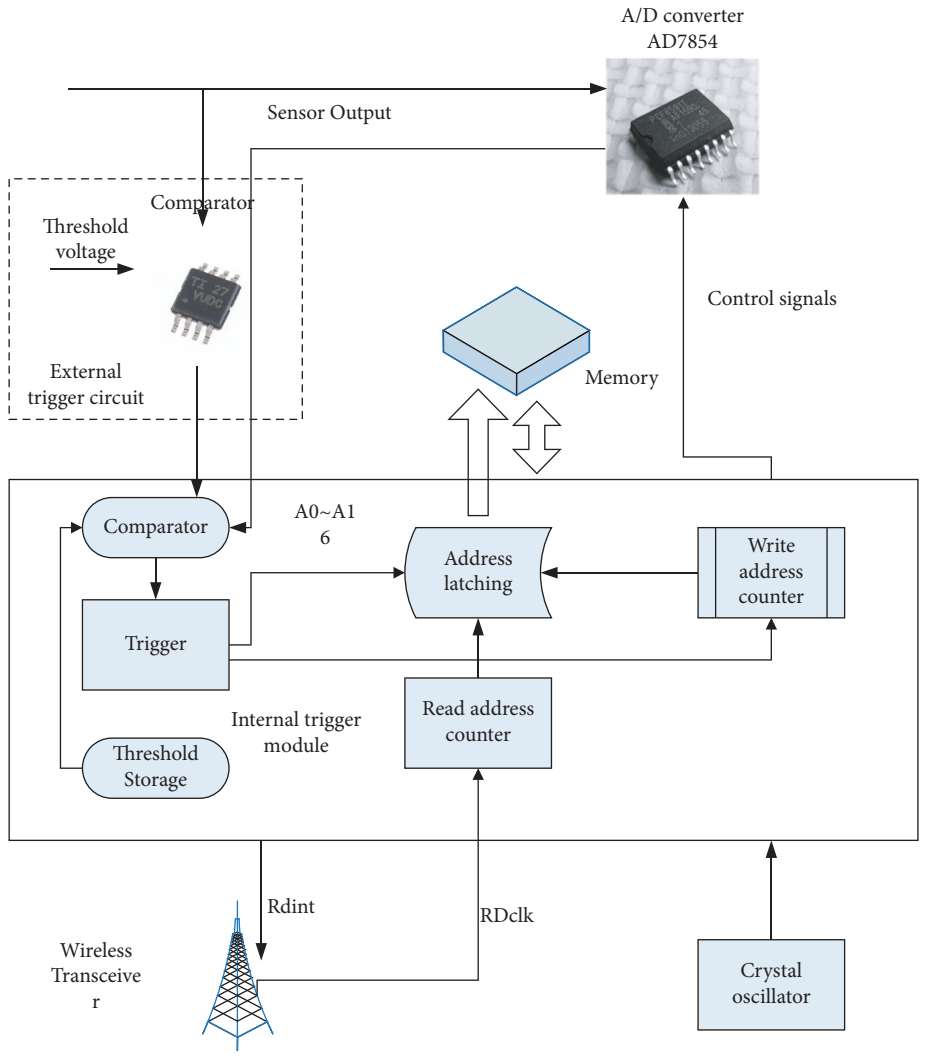

Figure 6: Schematic diagram of the hardware working principle of sensor network nodes.

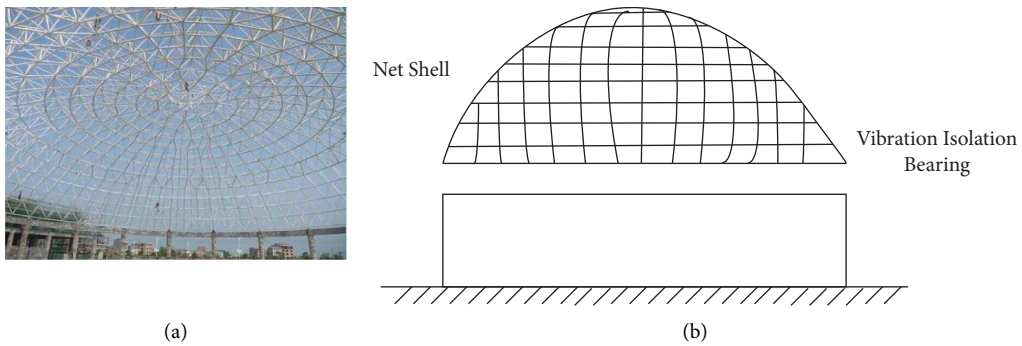

Figure 7: Double-layer spherical mesh shell structure model and arrangement scheme.

span ratio of 0.2, and a thickness of the reticulated shell of 2 meters, supported by the bottom chord. This structural model is shown in Figure 7(a). Five kinds of steel pipes (seamless Q235 steel pipes) of 114×6, 133×8, 140×7.5, 152×8, and 159×8 are used as reinforcement for the reticulated shell, and the roof load is assumed to be 1 kN/m^2. In the numerical simulation, the space element member model is used for all the stressed members of the reticulated shell. In order to ensure the overall rigidity of the reticulated shell structure, a steel box with a size of $0.8 \times 0.6 \times 0.05$ m is installed on the bottom support of the lattice window. For the multidimensional isolation condition, the isolation bearing is installed at the bottom of the box part of the reticulated shell frame structure, as shown in Figure 7(b).

Table 3: Seismic isolation bearing parameters.

Projects	Vibration isolation bearing parameters	Projects	Vibration isolation bearing parameters
Effective diameter (mm)	300	Equivalent horizontal stiffness (KN/m)	882
Height (mm)	105	Stiffness before yielding (KN/m)	3120
Equivalent damping ratio (%)	27.5	Stiffness after yielding (KN/m)	475

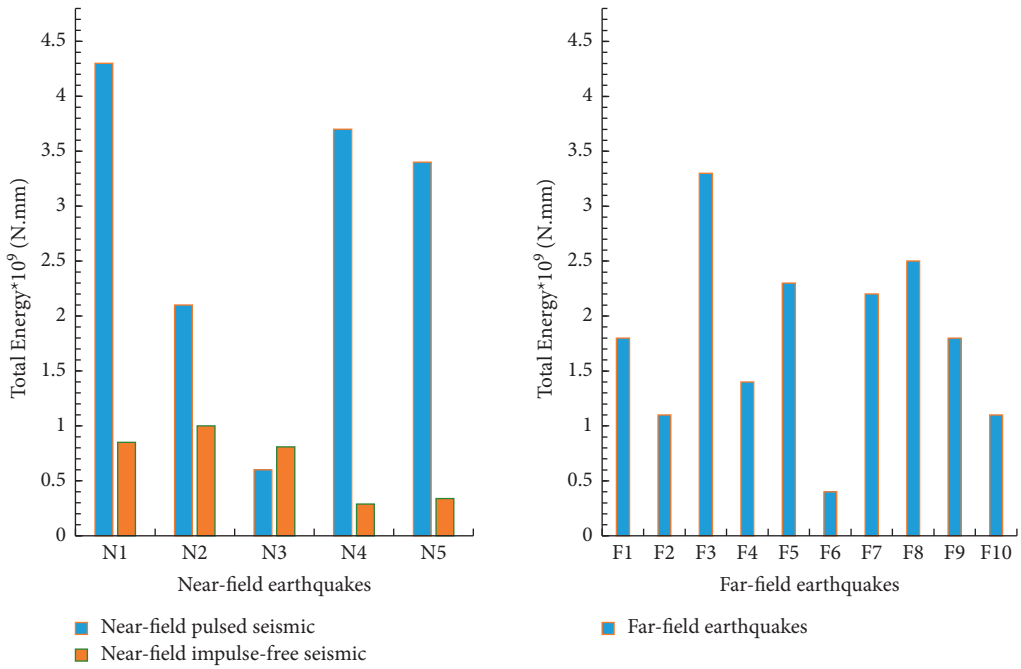

Figure 8: Earthquake energy input.

The load-bearing structure of the lower part of the reticulated shell is assumed to be a rigid structure, and its reinforcement for earthquake effects is not considered. Q345 steel is considered to be an ideal elastic-plastic material with a modulus of elasticity of $2.06 \times 10^5\,\mathrm{N/mm^2}$ and a mass density of $7850\,\mathrm{kg/m^3}$ according to the Von Mises yield criterion. The isolation bearing model was created in ABAQUS using C3D8R solid elements for the slider and base elements, while the reticulated shell uses quadratic interpolated Timoshenko beam elements B32 Sandwich beam elements. Simulations are performed with a coupling device. The material properties of the structural elements and reticulated shell structures are determined and coupled with the MSFB using contact and constraint functions to form the overall structural model.

The parameters of the seismic isolation bearings used are shown in Table 3.

5. Seismic Experimental Analysis of the Reticulated Shell Structure of the Isolation Bearing

Since near-field earthquakes and far-field earthquakes have different ground vibration characteristics, their effects on the seismic response of the structure are also very different. It was found that the seismic response of ground-isolated structures to near-field pulsations and far-field vibrations was analyzed in this paper. From Figure 8, it can be seen that the total energy of the ground isolation structure in the far field is greater than the total energy of the near-field unpulsed ground vibration but less than the total energy of the near-field ground vibration pulse. Therefore, the total energy of the basic isolation structure under the near-field pulse ground motion is the largest. That is to say, the seismic response of the basic isolation structure under the near-field pulse ground motion is the largest.

The seismic isolation bearing of the reticulated shell structure made of seismic isolation is placed between the foundation and the foot of the building and is separated by a seismic isolation layer so that more than 80% of the seismic energy cannot be transmitted to the superstructure, which effectively reduce the impact and damage of earthquakes on the overall structure or structural components. However, the failure of the isolation support impairs the ability to absorb seismic energy, which is reflected in the variation in the degree of ground energy dissipation at each height of the upper floors. As shown in Figure 9, for different seismic waves, the energy consumed by the seismic fortification is

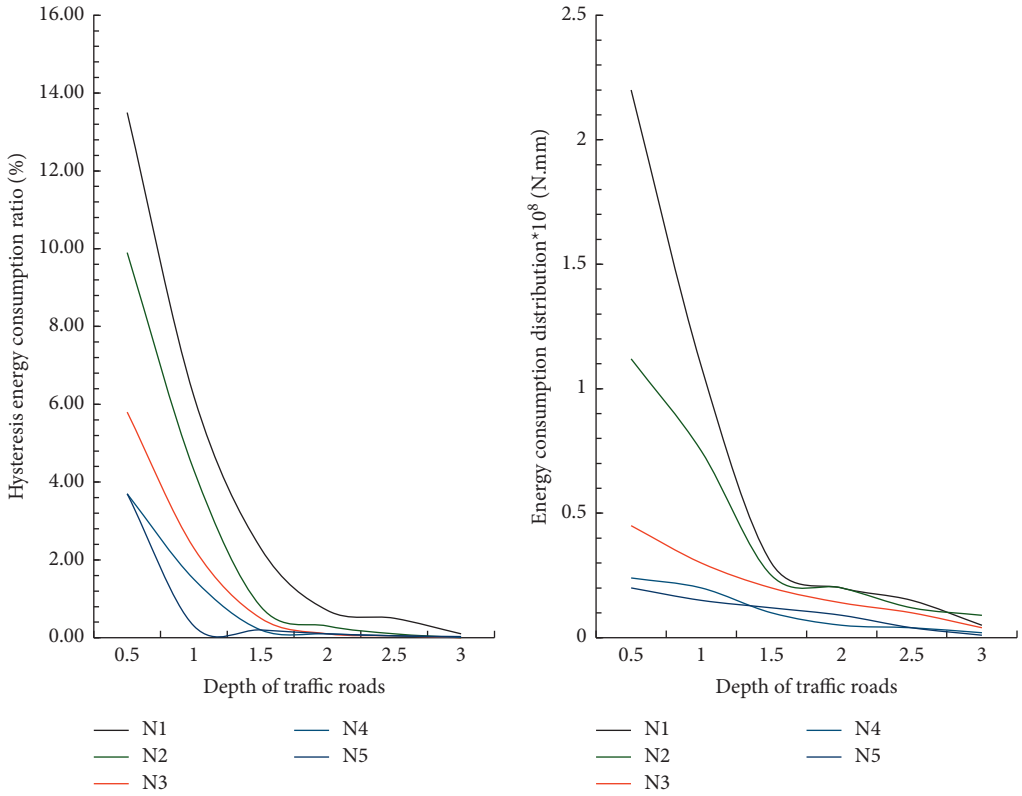

Figure 9: Energy consumption distribution of the reticulated shell structure of the isolation bearing.

Table 4: Mechanical performance parameters of isolation bearings.

Peak acceleration	0.01 g			0.02 g		
Vertical pressure (kN)	25	35	45	25	35	45
Equivalent stiffness (kN/mm)	1.186	1.674	2.140	0.981	1.24	1.401
Energy consumption per unit cycle (J)	200	341	410	420	658	942
Equivalent damping ratio	0.331	0.374	0.401	0.215	0.284	0.325

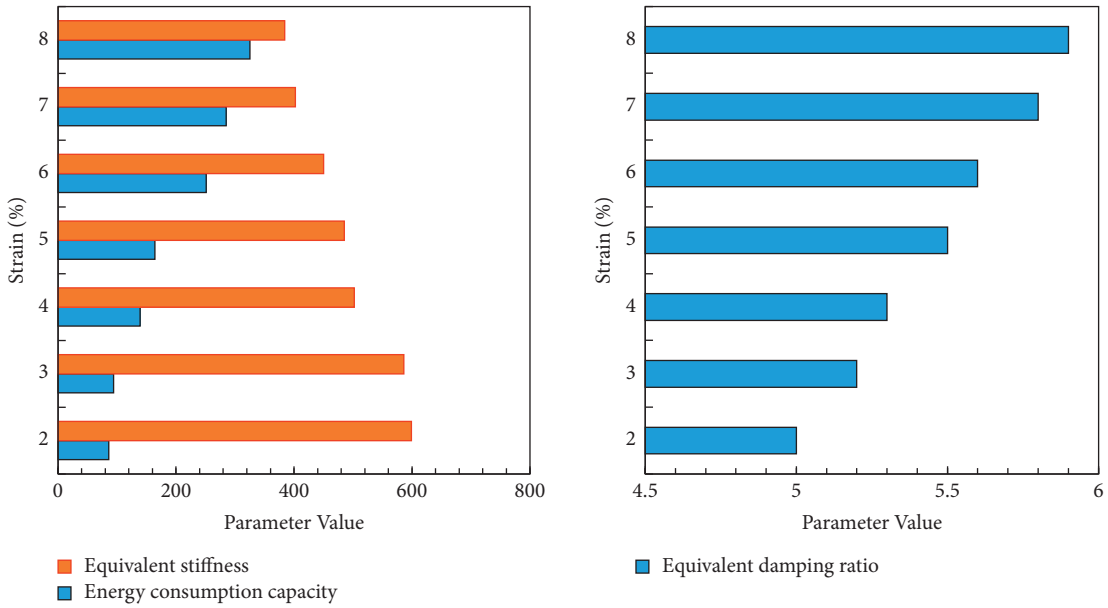

Figure 10: Cyclic loading test of isolation bearings.

different, but the hysteretic energy dissipation of the upper ground structure follows the principle of "upper low and lower higher". That is, the hysteretic energy dissipation of the superstructure decreases as the height increases, so the location of the first layer is a priority in the structural design. Therefore, the location of the ground floor is the focus of the structural design.

For a simple harmonic excitation performance test, the effect of changing the vertical stress on the hysteresis behavior of the bearing was investigated by changing the magnitude of the vertically applied force when a waveform with a sinusoidal function was introduced. Table 4 shows the values of three mechano-mechanical parameters, namely equivalent stiffness, energy loss per unit cycle, and equivalent damping ratio. Figure 10 depicts the cyclic loading test of the isolation bearing.

When the maximum acceleration increased from 0.01 g to 0.02 g, the equivalent stiffness and equivalent damping ratio of the isolation bearing decreased, while the energy dissipated per unit cycle increased significantly. At a given maximum acceleration, the equivalent stiffness and equivalent damping ratios dissipated per unit cycle increase with increasing vertical force.

6. Conclusion

Most earthquakes are not felt by humans because they are low in magnitude or occur in remote areas, but some earthquakes occur near us, and if the earthquake is strong, it can cause serious personal safety threats and economic losses. China is one of the countries in the world that has experienced many earthquakes and is greatly affected by earthquakes. Earthquakes are inherently random, and their mechanisms are complex and variable. Even though a lot of time and effort has been invested in earthquake prediction at home and abroad, there is still no significant effect. In order to reduce the number of victims caused by earthquakes, it is necessary to improve the seismic performance of building facilities and the ability to resist collapse caused by strong earthquakes so as to greatly reduce the losses caused by the collapse. The reticulated shell structure has both the force transmission characteristics of the rod system and the structural properties of the shell. The force is mainly transmitted point by point through the tension, pressure, or shear force in two directions in the shell, and the force transmission process is very clear. At this stage, the spatial reticulated shell structural system is a structural system with broad development prospects. In the optimization of seismic performance, this paper only studies the energy dissipation capacity of the reticulated shell structure of the seismic isolation bearing. The material selection of the isolation bearing and the shape of the bearing of the isolation bearing have not been studied, which is the deficiency of this paper.

Data Availability

Data sharing is not applicable to this article as no new data were created or analyzed in this study.

Conflicts of Interest

The authors state that this article has no conflicts of interest.

Acknowledgments

This work was supported by K1802006 (Science and technology research project of Suihua University) (Application Research on "Internet +" and building energy saving mode).

References

[1] Q. Wu, W. He, W. Liu, Y. Weixin, and Q. Chuan, "Large deformation hardening model of lead rubber bearings and elastic-plastic analysis for a structure with seismic isolation," *Zhendong yu Chongji/Journal of Vibration and Shock*, vol. 36, no. 15, pp. 90–97, 2017.

[2] X. Hong, W. Guo, and Z. Wang, "Seismic analysis of coupled high-speed train-bridge with the isolation of friction pendulum bearing," *Advances in Civil Engineering*, vol. 2020, no. 44, pp. 1–15, 2020.

[3] T. Hiraki, K. Kanazawa, and H. Kitamura, "Mechanical energy evaluation method for seismic isolation systems with rubber bearings under large deflection," *Journal of Structural and Construction Engineering (Transactions of AIJ)*, vol. 82, no. 731, pp. 75–85, 2017.

[4] A. Mohebbi, K. L. Ryan, and D. H. Sanders, "Seismic protection of the piers of integral bridges using sliding bearings," *Journal of Earthquake Engineering*, vol. 21, no. 7-8, pp. 1365–1384, 2017.

[5] X. Yan, Q. Ai, H. Mao, and X. Xiaoyong, "Multi-dimensional seismic response analysis of three-dimensional seismic-isolation mega-sub structure," *China Civil Engineering Journal*, vol. 50, no. 5, pp. 36–46, 2017.

[6] L. I. Qingning, M. Cheng, J. Yin, L. Yan, and X. Liao, "Analysis and experimental study on performance of curved bridge sliding seismic isolation," *World Earthquake Engineering*, vol. 33, no. 1, pp. 34–40, 2017.

[7] A. Mukherjee, D. K. Jain, P. Goswami, Q. Xin, L. Yang, and J. J. P. C. Rodrigues, "Back propagation neural network based cluster head identification in MIMO sensor networks for intelligent transportation systems," *IEEE Access*, vol. 8, no. 1, Article ID 28524, 2020.

[8] M. Mousa, K. Sharma, and C. G. Claudel, "Inertial measurement units-based probe vehicles: automatic calibration, trajectory estimation, and context detection," *IEEE Transactions on Intelligent Transportation Systems*, vol. 19, no. 10, pp. 3133–3143, 2018.

[9] Z. Liu and S. Zhang, "Artificial neural network-based method for seismic analysis of concrete-filled steel tube Arch bridges," *Computational Intelligence and Neuroscience*, vol. 2021, no. 2, pp. 1–10, 2021.

[10] M. A. Nabian and H. Meidani, "Deep learning for accelerated seismic reliability analysis of transportation networks," *Computer-Aided Civil and Infrastructure Engineering*, vol. 33, no. 6, pp. 443–458, 2018.

[11] H. Malik and W. Zatar, "Agent based routing approach to support structural health monitoring-informed, intelligent transportation system," *Journal of Ambient Intelligence and Humanized Computing*, vol. 11, no. 3, pp. 1031–1043, 2020.

[12] Y. Peng, X. Cao, Y. Chao, Z. Xiao, X. Xi, and D. Wu, "Proactive drone-cell deployment: overload relief for a cellular network under flash crowd traffic," *IEEE Transactions on*

Intelligent Transportation Systems, vol. 18, no. 10, pp. 2877–2892, 2017.

[13] M. Gao, W. Ping, C. Yong, R. Chen, and D. Cai, "Design and verification of a rail-borne energy harvester for powering wireless sensor networks in the railway industry," *IEEE Transactions on Intelligent Transportation Systems*, vol. 18, no. 99, pp. 1596–1609, 2017.

[14] Z. Zhang and S. Chen, "Real-time seam penetration identification in arc welding based on fusion of sound, voltage and spectrum signals," *Journal of Intelligent Manufacturing*, vol. 28, no. 1, pp. 207–218, 2017.

[15] C. Li, G. Zhang, Y. Mao, and X. Zhao, "A data aggregation privacy protection algorithm based on fat tree in wireless sensor networks," *Security and Communication Networks*, vol. 2021, no. 8, pp. 1–9, 2021.

[16] S. Salgadoe, F. Lu, and F. Lu, "An Anomaly Detection Model for Ultra Low Powered Wireless Sensor Networks Utilizing Attributes of IEEE 802.15.4e/TSCH," *Journal of Communications*, vol. 14, no. 5, pp. 335–341, 2019.

[17] T. Jinjun, W. Hua, W. Yinhai, L. Xiaoyue, and L. Fang, "Hybrid prediction approach based on weekly similarities of traffic flow for different temporal scales," *Transportation Research Record*, vol. 2443, no. 1, pp. 21–31, 2018.

[18] F. Chao, Z. He, R. Feng et al., "Predictive trajectory-based mobile data gathering scheme for wireless sensor networks," *Complexity*, vol. 2021, no. 2, pp. 1–17, 2021.

[19] W. Zhou, J. S. Berrio, S. Worrall, and E. Nebot, "Automated evaluation of semantic segmentation robustness for autonomous driving," *IEEE Transactions on Intelligent Transportation Systems*, vol. 21, no. 5, pp. 1951–1963, 2020.

[20] W. Yang, X. Sun, M. Wang, and P. Liu, "Vertical stiffness degradation of laminated rubber bearings under lateral deformation," *Construction and Building Materials*, vol. 152, no. oct.15, pp. 310–318, 2017.

[21] D. Wang, Y. Zhang, C. Wu, X. Guofeng, and H. Wencheng, "Seismic performance of base-isolated AP1000 shield building with consideration of fluid-structure interaction," *Nuclear Engineering and Design*, vol. 353, Article ID 110241.1, 2019.

[22] W. He, Y. Huang, and W. Liu, "Seismic responses of a nuclear plant isolated structure supported by rubber bearings with a multi-factor coupled mechanical model," *Zhendong yu Chongji/Journal of Vibration and Shock*, vol. 37, no. 17, pp. 72–78, 2018.

[23] Q. Han, B. Wang, and J. Jia, "Seismic response analysis of isolated offshore bridge with friction sliding bearings," *Earthquakes and Structures*, vol. 16, no. 6, pp. 641–654, 2019.

[24] T. Yamauchi, H. Kitamura, M. Nagano et al., "Study on application of seismic deformation method for pile top seismic isolation buildings," *Journal of Structural and Construction Engineering (Transactions of AIJ)*, vol. 83, no. 743, pp. 69–79, 2018.

[25] Y. Shi, J. M. Xuan, J. Yao, and Z. -Y. Zhang, "Analysis of seismic performance of long span rail transit bridge," *Bridge Construction*, vol. 47, no. 6, pp. 42–47, 2017.